CrystEngComm

ROYAL SOCIETY OF CHEMISTRY

PAPER

View Article Online
View Journal

Check for updates

Cite this: DOI: 10.1039/d6ce00065g

Received 23rd January 2026,
Accepted 7th May 2026

DOI: 10.1039/d6ce00065g

rsc.li/crystengcomm

The impact of polymorphism on the thermophysical properties of methyl behenate as a phase-change material

Rebecca Ravotti, *[ab] Xiaojiao Liu,[b] Colin R. Pulham [b] and Anastasia Stamatiou[a]

Polymorphism plays a critical role in determining the performance of bio-derived phase-change materials (PCMs). In this work, we investigate the polymorphism of methyl behenate, a fatty acid ester with potential as a sustainable phase-change material for thermal energy storage. Three previously unknown polymorphs were identified, and their thermophysical properties were characterised by differential scanning calorimetry and hot-stage microscopy, highlighting the strong influence of polymorphism on the material properties. The structure of two polymorphs were determined using laboratory and synchrotron powder X-ray diffraction. The comparison with a related fatty acid ester reveals common structural trends, suggesting emerging structure–property relationships within this class of materials. These results provide new insights into ester-based PCMs and support the rational design of sustainable thermal energy storage materials.

1 Introduction

In the light of the current energy crisis and growing levels of fuel poverty, it is crucial to increase the proportion of renewable energy in the energy mix to achieve the Paris Agreement targets set for 2030 and 2050.[1] Thermal energy storage (TES) and particularly latent heat storage (LHS) are vital technologies for reaching these goals, especially in urban areas where space efficiency is essential. The use of phase-change materials (PCMs) for heat storage is an attractive solution that is becoming more common.[2]

Both organic and inorganic materials are used as PCMs, and materials such as salt hydrates have gained attention because of their availability, low cost, and high volumetric energy densities.[3] However, organic materials offer benefits that include: derivation from biomass or waste streams; consistent thermophysical properties; reduced tendencies both to supercool and to melt incongruently resulting in phase segregation.[4] In particular, esters, formed from carboxylic acids and alcohols, show high enthalpies of fusion, a wide range of melting points, and are naturally abundant in oils and waxes.[5–8] Linear saturated fatty acid methyl esters (FAME) have been identified as particularly promising, with enthalpies of fusion in the range 180–200 J g^{-1}, and a higher stability to degradation compared to esters derived from longer-chain alcohols. Examples of fatty acid methyl esters as PCMs include methyl myristate, methyl palmitate and methyl stearate.[6,9,10]

Some PCMs exhibit polymorphism, which is the ability of a compound to crystallise in different structures while maintaining the same chemical composition.[11] Although this phenomenon is often associated with organic materials, according to Cruz-Cabeza *et al.*, over 40% of organic compounds are likely to exhibit polymorphism.[12] This significantly affects the design of LHS systems because the thermophysical properties, such as melting point and enthalpy of fusion, can vary between polymorphic forms. Understanding and controlling polymorphism is essential to consistently produce the desired form. Despite its importance, polymorphism is often overlooked in the TES field, with only limited information available on PCMs such as paraffins and fatty esters.[13]

Although the polymorphism of triglycerides (esters of glycerol and three fatty acid molecules) is well-documented,[7,14–20] fewer studies have been reported for linear saturated fatty esters formed from a mono-alcohol and a fatty acid, *i.e.* RCOOR′. In 1961, Lutton and Hugenberg[21] reported the polymorphism of methyl- and ethyl-substituted palmitates and stearates and their mixtures, noting the existence of two forms (α and β) with only slight differences in melting points. In a more recent study, Liu *et al.*[22] reported five different forms of methyl stearate prepared under a range of temperature conditions. Cabus *et al.*[23] investigated polymorphism in fatty diesters, while Soodoo *et al.*[24] examined fatty terephthalates and methods to control polymorphism by addition of aromatic derivatives by increasing the torsional energy barrier.

---

[a] *HSLU Lucerne University of Applied Sciences, Technikumstrasse 21, Horw CH-6048, Switzerland. E-mail: rebecca.ravotti@hslu.ch*
[b] *EaStChem, University of Edinburgh, School of Chemistry, David Brewster Rd., Edinburgh EH9 3FJ, UK*

Methyl behenate is a FAME derived from behenic acid, a long-chain saturated fatty acid found in sources such as grapeseed and peanut oils.[25] In a previous study,[6,9] we identified methyl behenate (MEBE) as a promising PCM for temperature applications in the 45–55 °C range (such as photovoltaic and thermoelectric,[26] or domestic and small district water heating[27]), where very few other inorganic or organic PCMs are typically available.[28] To date, to the best of our knowledge this is the only study evaluating MEBE as a PCM and investigating its thermophysical properties. The chemical structure of MEBE is shown in Fig. 1.

No information has been found on the polymorphism of methyl behenate either as structural information and published structures or as calorimetry data. A few studies have focused on the polymorphism of glyceryl behenates and behenic acid as they are widely used in pharmaceutical formulations,[29–31] but none has mentioned polymorphism concerning fatty acid esters of behenic acid.

In this study, the polymorphism of MEBE was explored using differential scanning calorimetry (DSC), single crystal and powder X-ray diffraction (XRD), and hot-stage microscopy (HSM). Three different polymorphic forms – form I, form II, and form III – were identified, and the crystal structures and thermal properties of forms I and III were determined for the first time. This provides a deeper understanding of the polymorphism of MEBE and opens the door to future research on systematically controlling the polymorphic behaviour of fatty esters.

2 Materials and methods

2.1 Materials

All reagents were obtained from Merck and used as received, without further purification. Methyl behenate was purchased as an analytical standard with purity ≥ 99.0%. Ethyl acetate (≥99.7%, suitable for HPLC) and methanol (≥99.9%, HPLC Plus) were used to grow single crystals of MEBE.

2.2 Differential scanning calorimetry

The phase-change temperatures (T_m and T_c) and enthalpies of fusion (ΔH) were measured on a DSC 823e and a DSC 3+ (METTLER TOLEDO, Greifensee, CH) with robotic autosamplers. The heating and cooling regime outlined in Fig. A1 (in the SI) was employed. T_m and T_c were calculated using the tangent method.[32] ΔH was derived by integration of the area beneath the peak of the thermal event. The DSC instrument was calibrated with an indium standard, and the uncertainty in the temperatures is reported by the manufacturer as ±0.1 K. All measurements were repeated three times and were conducted under a constant flow of nitrogen at a rate of 50 mL min^{-1}, and sample masses were typically between 5 and 10 mg. Data were analysed using the METTLER TOLEDO STARe software (v.16.20).

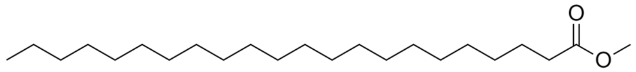

Fig. 1 Chemical structure of methyl behenate (MEBE).

2.3 Hot-stage microscopy (HSM)

A custom-built heating/cooling stage from the Lucerne University of Applied Sciences and Arts (HSLU) was used, combined with a DinoLite AM73915MZT with polarized backlight BL-ZW1. The microscope features 8 LEDs, a magnification range of 10–220×, and a resolution of 5 megapixels. The stage (see Fig. A2 in the SI), built according to Meerstetter Engineering's guidelines, includes a Peltier element (Peltron 125 A 0020 H200 CH 4,7 S), a TEC controller with a built-in PID controller (Meerstetter Engineering TEC-1091), a PT100 temperature sensor, a heatsink (Fischer Elektronik ICK S 50 × 50 × 25) with a radial fan (NMB Minebea BG0703-B055-000-00), and a power supply. The stage is operated using Meerstetter Engineering software, with a built-in autotune feature for adjusting PID values, allowing temperature control within ±0.01 K.

Samples of MEBE were cycled on the HSM under polarized light with two consecutive cycles between 30 and 70 °C, using heating/cooling rates of 10 and 1 K min^{-1}. Five-minute isotherms were included at the start and end of each cycle to stabilise heat flow and temperature, similar to DSC methodologies (Fig. A1 in the SI).

The HSM was calibrated using a sample of methyl palmitate from Sigma Aldrich, and all experiments were conducted with a coverslip over the sample on the microscope slide. Details on the calibration results can be found in Table S1 in the SI, showing a good degree of agreement between the two techniques.

2.4 Single crystal X-ray diffraction

Unit-cell parameters were obtained using the CrysAlisPro[33] program, and Olex 2 (ref. 34) was used for structure determination. The single crystals were mounted on a single crystal XRD – Rigaku Oxford Diffraction SuperNova diffractometer (Cu-Kα radiation, λ = 1.5418 Å). The structures were solved with the ShelXT[35] program using intrinsic phasing methods. Refinements were performed with the ShelXL[36] program using least-squares minimisation. Topas (v6 Academic)[37] was used to perform Pawley refinements.[38]

2.4.1 Growth of single crystals from solution. Single crystals of MEBE were obtained by vapour diffusion using ethyl acetate as a solvent and methanol as an antisolvent.

MEBE was dissolved in ethyl acetate (EtOAc) to form a saturated solution in a glass vial with a diameter of 1.5 cm and length of 5 cm. The vial was then placed inside a bigger glass vial filled to about 1/4 of the volume with methanol (MeOH). The bigger vial was sealed with a lid and Parafilm™ and placed on a shelf far from sources of disturbance or vibrations at 23–24 °C (see Fig. A3 in the SI). After 4–7 days, rhombohedral, plate-like, thin crystals were formed. A suitable single crystal was selected and mounted on the single crystal XRD instrument, and data collection was conducted at 24 °C.

2.4.2 Growth of single crystals from the melt. A sample of MEBE was finely ground to give a polycrystalline powder and loaded into a 0.7 mm borosilicate capillary, which was mounted on the single crystal XRD instrument. Initially, the sample was heated to 77 °C at 6 K min^{-1} in order to melt the sample, and then slowly cooled to −3 °C at 0.17 K min^{-1}. The quality of data recorded at −3 °C was poor, and so it was further cooled to −53 °C at a rate of 6 K min^{-1}. Data collection was conducted at −53 °C.

2.5 Powder X-ray diffraction

Powder patterns were recorded on a Bruker D8 diffractometer (Cu-Kα radiation, λ = 1.5418 Å) with a Lynxeye (1D mode) detector and an Oxford Cryostream for temperature control. A sample of MEBE was loaded into a 0.7 mm borosilicate capillary with no prior grinding. The capillary was then mounted on the diffractometer and the patterns were recorded between 5 and 50° (2θ) with a 2θ increment of 0.015° and 0.7 s per step. Data were collected after stabilising for 30 min.

Powder diffraction patterns of MEBE were also recorded on the I11 beamline at the Diamond Light Source, Harwell (UK) with λ = 0.824429 ± 0.000001 Å. The patterns were collected between 2θ = 2 and 80° with a collection time of 30 s per pattern while heating/cooling between 24 and 70 °C using rates of ∼1 K min^{-1}.

3 Results

3.1 DSC studies

3.1.1 DSC cycling of MEBE. In order to better understand the thermodynamic behaviour of MEBE, the commercially-supplied samples of MEBE were cycled in a DSC instrument over two consecutive heating/cooling cycles between 20 and 80 °C at different rates (10, 1, and 0.1 K min^{-1}) using the methodology shown in Fig. A1 in the SI. The results obtained are shown in Fig. 2. All calorimetry data for the three polymorphic forms are summarised in Table 1 (onset *T*) and in Table 2 (Δ*H*).

The curves measured at 1 K min^{-1} are considered first (Fig. 2B). During the first heating cycle (purple curve), a broad peak was observed with an onset melting temperature (T_m) ∼ 53.7 °C and Δ*H* ∼ 221 J g^{-1} corresponding to melting of the crystalline form present in the commercial sample.

On cooling (dark blue curve), two exothermic peaks were observed; the first is broad with an onset crystallisation temperature (T_c) of ∼50.4 °C followed by a much sharper peak at T_c ∼ 49.5 °C, with a combined Δ*H* ∼ 207 J g^{-1}. This suggests that two different polymorphic forms crystallised consecutively.

During the second heating cycle (light blue curve), a single, broad peak was observed with an onset T_m of ∼52.1 °C and a Δ*H* of ∼209 J g^{-1}.

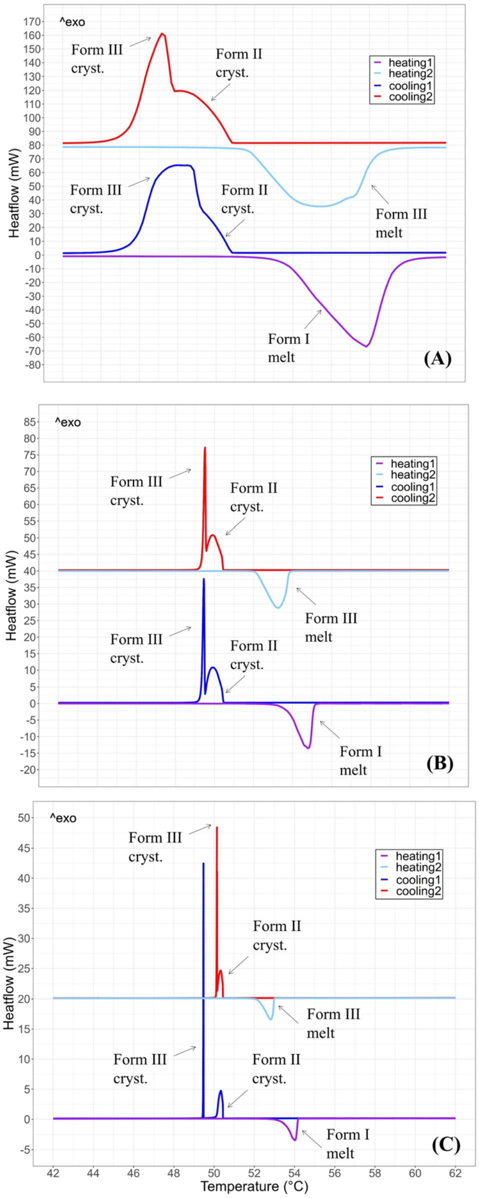

Fig. 2 DSC traces showing the thermal behaviour of MEBE at three different heating rates: 10 K min^{-1} (A), 1 K min^{-1} (B), and 0.1 K min^{-1} (C).

During the second cooling cycle (red curve), the same crystallisation behaviour was apparent *i.e.* two exothermic peaks were observed at identical temperatures.

For the second heating cycle, the lower values of both T_m and Δ*H* compared to those of the first heating cycle imply that crystallisation from the melt results in the formation of different polymorphs.

Using a fresh sample of MEBE, similar results were obtained at the slower ramp rate of 0.1 K min^{-1} (Fig. 2C). On the first heating cycle (purple curve), the sample melted again at a higher temperature (T_m ∼ 53.2 °C; Δ*H* ∼ 200 J g^{-1}) compared to the second cycle (light blue curve, T_m ∼ 52.3 °C; Δ*H* ∼ 192 J g^{-1}), and during both cooling cycles two distinct exothermic peaks were observed, with one being broad (T_c ∼ 50.5 °C) and the other much sharper (T_c ∼ 49.5 °C), with a

Table 1 Overview of onset T_m and T_c [°C] of each phase transformation

Onset T [°C]	10 K min^{-1}	1 K min^{-1}	0.1 K min^{-1}
1st cycle			
Form I melting	53.4 ± 0.1	53.7 ± 0.1	53.2 ± 0.7
Form II crystallisation	50.8 ± 0.1	50.4 ± 0.1	50.4 ± 0.1
Form III crystallisation	48.8 ± 1.1	49.5 ± 0.3	49.5 ± 0.7
2nd cycle			
Form III melting	51.6 ± 0.1	52.1 ± 0.1	52.3 ± 0.1
Form II crystallisation	50.8 ± 0.1	50.4 ± 0.1	50.4 ± 0.1
Form III crystallisation	48.3 ± 1.0	49.3 ± 0.4	49.5 ± 0.1

Table 2 Overview of ΔH [J g^{-1}] of each phase transformation

ΔH [J g^{-1}]	10 K min^{-1}	1 K min^{-1}	0.1 K min^{-1}
1st cycle			
Form I melting	226 ± 2	221 ± 11	200 ± 36
Form II + form III crystallisation	209 ± 2	207 ± 9	191 ± 33
2nd cycle			
Form III melting	213 ± 2	209 ± 10	192 ± 34
Form II + form III crystallisation	210 ± 2	206 ± 10	191 ± 34

combined value of $\Delta H \sim 191$ J g^{-1}. Interestingly the separation between these crystallisation peaks varied randomly between cycles over a range of $\sim\Delta T = 1$–2 °C.

Similar behaviour was observed at the fastest ramp rate of 10 K min^{-1} (Fig. 2A) and with a fresh sample of MEBE. All peaks were substantially broader because of the faster heating rate. On the first heating cycle (purple curve), $\Delta H \sim 226$ J g^{-1} was recorded. During the first cooling cycle (dark blue curve) a combined $\Delta H \sim 209$ J g^{-1} associated with crystallisation was recorded, consistent with complete melting in the second cycle (light blue curve), $\Delta H \sim 213$ J g^{-1}.

Based on these observations, the hypothesis is that the crystal form found in the commercially available sample of MEBE (and hereafter referred to as form I) melts at $T_m \sim 53.5$ °C. On cooling the melt, some supercooling is observed before the onset of crystallisation into a second form (form II) at $T_c \sim 50.4$ °C. On further cooling, form II transforms into a third form (form III) at $T_c \sim 49.5$ °C. On subsequent heating, form III then melts at $T_m \sim 52.3$ °C. Based on its lower T_m and lower ΔH compared to form I, form III is thermodynamically less stable than form I. The intermediate form II produced from the melt appears to have only a very limited stability range and transforms rapidly to form III on cooling below ~49 °C. At cooling rates of 10 and 1 K min^{-1}, the crystallisation of form II is incomplete before subsequent crystallisation of form III. This suggests that form III recrystallises from the melt. In contrast, at 0.1 K min^{-1} the crystallisation of form II appears to be complete, and therefore the crystallisation of form III is likely through a solid–solid transformation. The larger uncertainty in the enthalpy of fusion at 0.1 K min^{-1} is attributed to increased experimental noise at slower heating rates. A minor secondary peak was occasionally observed during the subsequent melting of form III, which may indicate only a partial solid–solid transformation during crystallisation. However, as the crystallisation and melting enthalpies are in good agreement, this remains unclear and would require further investigation.

3.1.2 DSC cycling of single crystals of MEBE. Fig. 3 shows rhombohedral, thin, plate-like crystals of MEBE that were obtained by vapour diffusion of methanol into a saturated solution of MEBE in ethyl acetate at 24 °C. The single crystals obtained were studied using the DSC over five consecutive heating/cooling cycles between 20 and 80 °C at 1 K min^{-1}. The resulting data are shown in Fig. 4, while the average onset T_m and T_c, and average ΔH are summarised in Table 3.

The DSC plots shown in Fig. 4 were very similar to those for the commercial sample (Fig. 2). In the first heating cycle (endothermic, dark blue curve), form I melts at ~53.6 °C. During the initial cooling (exothermic, dark blue curve), form II crystallizes slowly at ~50.1 °C, followed by a rapid recrystallisation into form III at ~49.5 °C. Upon reheating (endothermic, red curve), form III melts at ~52.1 °C. This behaviour is consistent in all subsequent heating/cooling cycles (purple, light-blue, and yellow curves). This indicates that form I can be obtained by recrystallisation from solution whereas form III is produced from cooling the melt, *via* the metastable form II.

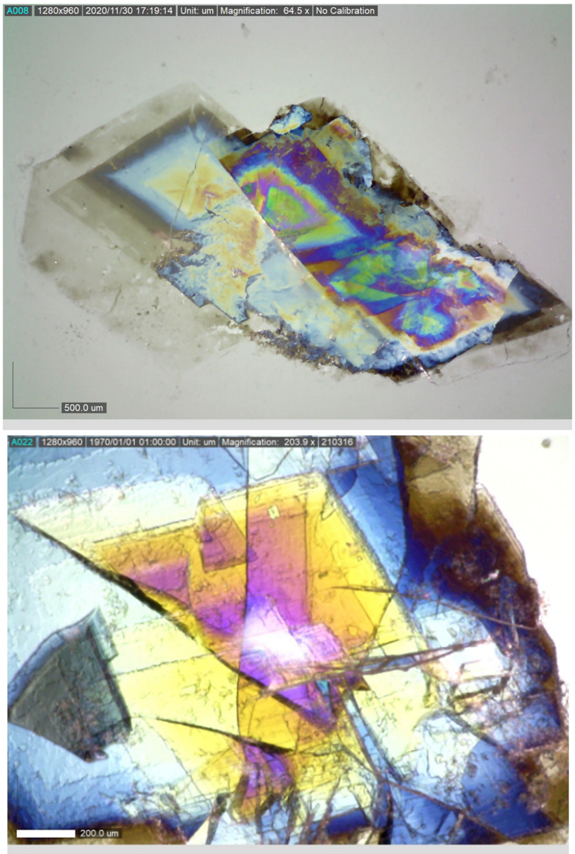

Fig. 3 Top) Thin plate-like single crystals of MEBE obtained *via* vapour diffusion. Bottom) Zoomed section.

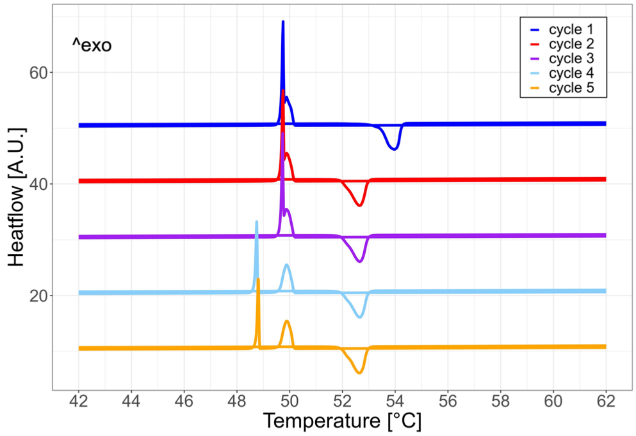

Fig. 4 DSC profile of MEBE single crystals obtained *via* vapour-diffusion in ethyl acetate with methanol.

3.1.3 Hot-stage microscopy studies. Hot-stage microscopy (HSM) studies were conducted to replicate the DSC investigation by cycling samples of MEBE twice between 30 °C and 70 °C at heating/cooling rates of 10 and 1 K min^{-1}, using the methodology from Fig. A1 in the SI. A rate of 0.1 K min^{-1} was not achievable with the HSM's heating/cooling stage. We defined T_0 as the earliest temperature at which a change in the sample was observed during melting or crystallisation. This broadly correlates with T_m and T_c from the DSC. An overview of the T_0 for each polymorphic form is provided in Table 4, while optical images of the key events from the HSM cycling tests are shown in Fig. 5 and 6.

Table 3 Overview of average onset T_m and T_c [°C] and ΔH [J g^{-1}] of single crystal MEBE cycled five times in the DSC at 1 K min^{-1}

1 K min^{-1}		
	T [°C]	ΔH [J g^{-1}]
Form I melting	53.6	211
Form II + form III crystallisation	50.1 ± 0.1	199 ± 1
Form III melting	52.1 ± 0.1	200 ± 1

At the start of the experiment, the commercial sample appeared as stacked plate-like crystals characteristic of form I (Fig. 5).

Upon heating at both 10 and 1 K min^{-1} (Fig. 5), form I began to melt at $T_0 \sim 51.5$ °C.

On cooling at 10 K min^{-1} (Fig. 6), transparent needle-like crystals appeared at $T_0 \sim 51.0°$ and grew slowly over a period of 10 seconds. On cooling at 1 K min^{-1} (Fig. 7), similar crystals appeared at $T_0 \sim 50.5$ °C but grew over a period of 70 seconds. Shortly afterwards, at both heating rates feather-like crystals initially formed on top of the needles at ~48.9 °C (10 K min^{-1}) and at ~49.5 °C (1 K min^{-1}); within ≤ 1 second the whole sample adopted this morphology. Correlation of these observations (onset T, crystal growth rates) with the results of the DSC studies strongly suggests that the needle-like crystals are associated with form II, and the feather-like crystals are associated with form III.

During the second heating cycle (Fig. 8), the feather-like crystals (form III) melted at $T_0 \sim 49.8$ °C (10 K min^{-1}), and at $T_0 \sim 50.7$ °C (1 K min^{-1}). This, combined with the observation of only a single endothermic transition in the DSC plot, suggests that form II is metastable and transforms into form III completely upon cooling.

The second cooling cycle showed identical crystallisation behaviour to the first cycle, again consistent with DSC experiments.

3.2 X-ray diffraction investigation

3.2.1 Form I. The crystal structure of form I was determined from X-ray data collected at 24 °C on a single crystal grown *via* vapour diffusion in ethyl acetate with methanol, as described in 2.4.1. Attempts to record data at lower temperatures (below −50 °C) resulted in substantial deterioration of data quality, most likely caused by a phase transition. However, due to the limited crystallinity of the low temperature form, the quality of the diffraction data was insufficient for structural characterisation. The collection of data at the relatively high temperature of 24 °C, combined with the motion of the long alkyl chains resulted in an unusually high *R*-factor (15.05%, see Table 5) for the structure. Despite

Table 4 Overview of onset T_0 [°C] of each phase transformation from the HSM, and comparison with the respective T_m [°C] from the DSC

Onset T_0 [°C] (HSM)			Onset T_m [°C] (DSC)	
	10 K min^{-1}	1 K min^{-1}	10 K min^{-1}	1 K min^{-1}
1st cycle				
Form I melting	51.4 ± 0.4	51.6 ± 0.3	53.4 ± 0.1	53.7 ± 0.1
Form II solidification	51.0 ± 0.4	50.5 ± 0.1	50.8 ± 0.1	50.4 ± 0.1
Form III solidification	48.9 ± 0.9	49.5 ± 0.3	48.8 ± 1.1	49.5 ± 0.3
2nd cycle				
Form III melting	49.8 ± 1.1	50.7 ± 1.1	51.6 ± 0.1	52.1 ± 0.1
Form II solidification	51.0 ± 0.4	50.5 ± 0.1	50.8 ± 0.1	50.4 ± 0.1
Form III solidification	48.3 ± 1.1	49.4 ± 0.4	48.3 ± 1.0	49.3 ± 0.4

the high *R*-factor, some useful structural information can be obtained. Form I crystallises in the orthorhombic system with space group $Pna2_1$. The asymmetric unit contains two independent molecules parallel to the *ab*-plane, tilted with respect to the *bc*-plane, differing in the conformations of the ester groups.

Fig. 9 shows the orientation of the molecules in the asymmetric unit and the unit cell as viewed along different axes. A complete list of bond lengths and angles can be found in the SI (Tables S2 and S3).

The C–O–C–O torsion angle is 17.30° in one molecule and −6.87° in the other. The unit cell comprises four molecules arranged as bilayers, with molecules within the layers arranged in an alternating head-to-head and tail-to-tail manner (see Fig. 9, bottom), similar to form III of methyl stearate described by Liu *et al.*[22]

3.2.2 Form III. The crystal structure of form III was solved from a single crystal grown from the melt in a glass capillary as described in 2.4.2.

The structure was initially indexed to the $P2_1/c$ space group. However, it exhibited approximately 49.8% whole-molecule disorder, corresponding to a flipped orientation about an inversion centre located at the molecular centroid. To account for this, the symmetry was increased to $C2/c$ by constraining the disorder to 50% and by setting the occupancy of the ester group as 0.5 for each side of the molecule. Hence, the asymmetric unit contains only half of a molecule, analogous to the behaviour of form IV of methyl stearate.[22]

Fig. 10 shows the orientation of the molecules in the asymmetric unit and the unit cell as seen from different axes.

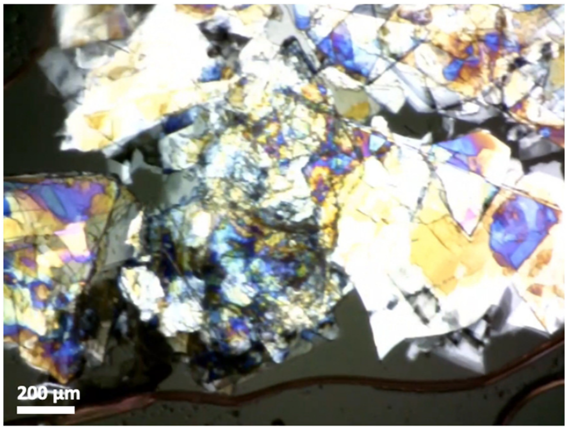

Fig. 5 Plate-like crystals of form I undergoing melting during the first heating cycle on the HSM.

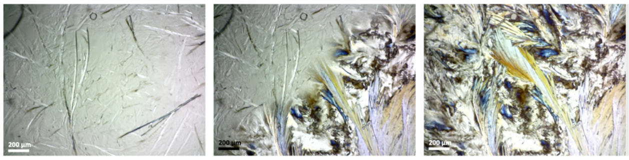

Fig. 6 Crystallisation of MEBE at a cooling rate of 10 K min^{-1}. Left) Crystals of form II appearing from the melt. Middle) Form III starting to crystallise on top of form II. Right) Form III completely crystallised on form II.

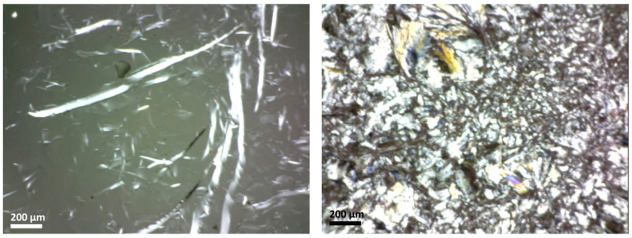

Fig. 7 Crystallisation behaviour of MEBE at a cooling rate of 1 K min^{-1}. Left) Crystals of form II appearing from the melt. Right) Form III completely crystallised on top of form II.

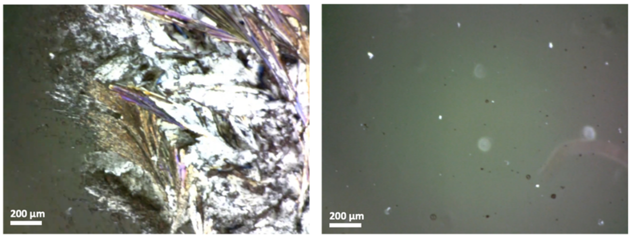

Fig. 8 Melting of MEBE at 10 K min^{-1} during the second heating cycle. Left) Onset melting of form III. Right) Form III completely melted.

Table 5 Overview of crystallographic information of MEBE polymorphs. As form II was not isolated, it was not possible to solve its crystal structure

	Form I	Form III
Space group	Orthorhombic $Pna2_1$	Monoclinic $C2/c$
Temperature [°C]	24	−53
a [Å]	5.6024 (3)	57.3935 (16)
b [Å]	7.3657 (6)	7.2578 (3)
c [Å]	113.5210 (7)	5.5616 (2)
α [°]	90	90
β [°]	90	97.0560 (3)
γ [°]	90	90
V [Å^3]	4684.50 (5)	2299.14 (14)
Z	8	4
Z'	2	0.5
R_1	15.05%	6.60%

A complete list of bond lengths and angles can be found n the SI (Tables S4 and S5).

MEBE molecules pack in oblique layers parallel to the crystallographic *ac* plane, but tilted with respect to the *bc* plane. The unit cell contains two molecular layers disordered around the molecular centre of inversion. Hydrogen atoms in the proximity of the ester group also appear to be disordered, similar to form IV of methyl stearate.[22]

There is also evidence of disorder in the ester group, with an apparent bond angle of 115.6°, similar to form III of methyl stearate.[22]

Both form IV of methyl stearate and form III of MEBE were obtained directly by cooling from the melt. Despite the difference in carbon number (C19 for methyl stearate, C23 for MEBE), both form very similar unit cells with the only difference being a longer *a* axis and a wider *β* angle for MEBE, caused by the longer carbon chain. Table 5 summarises the crystallographic information of form I and form III. A comparison of the packing arrangements of form I and form III are seen in Fig. 11.

3.2.3 Form II. Despite multiple attempts to grow single crystals of form II from the melt, on all occasions rapid transformation to form III was observed, highlighting the metastability of form II. This metastability also prevented the formation of a phase-pure polycrystalline sample of form II. However, some evidence of form II was observed during *in situ* experiments using the Bruker D8 XRD instrument while cooling from the melt at 1 K min^{-1} to 49.0 °C and holding for 30 min as described in 2.5. Fig. 12 shows the powder patterns collected during cooling together with the powder patterns of form I and form III collected at 24 °C.

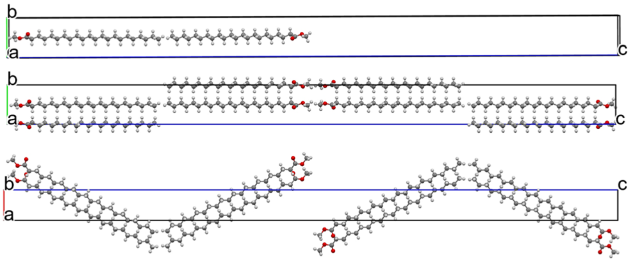

Fig. 9 Packing plot of form I of MEBE. Top) Asymmetric unit viewed from the crystallographic *a*-axis. Middle) Unit cell viewed from the crystallographic *a*-axis. Bottom) Unit cell viewed from the crystallographic *b*-axis.

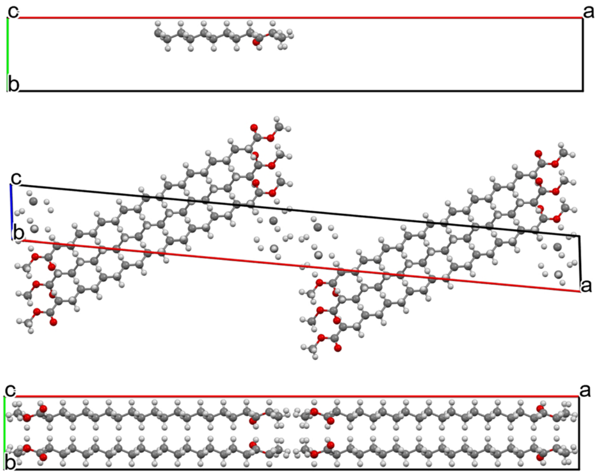

Fig. 10 Packing plot of form III of MEBE. Top) Asymmetric unit viewed from the crystallographic *c*-axis. Middle) Unit cell viewed from the crystallographic *b*-axis. Bottom) Unit cell viewed from the crystallographic *c*-axis.

A mixture of both form II and form III crystallised from the melt at T_c ~ 49.0 °C. Low-intensity peaks attributable to form II were observed at values of 2θ = 5.5, 8.25, 31.4 and 37.9°, together with peaks characteristic of form III. Peaks from form II disappear at ~48.8 °C, leaving only the pattern of form III. This is consistent with both DSC and HSM experiments, which highlighted the very limited temperature range of stability of form II.

3.3 Synchrotron powder X-ray diffraction studies

In situ synchrotron PXRD studies under dynamic heating/cooling conditions have been conducted using the beamline I11 at the Diamond Light Source. Here, a sample of commercial MEBE was first loaded into 0.5 mm borosilicate

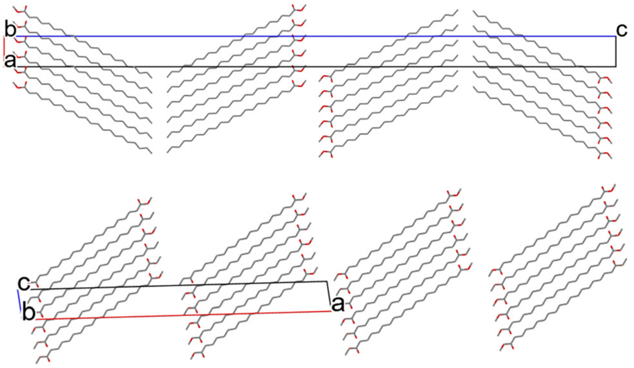

Fig. 11 Comparison between the packing behaviour of form I (top) and form III (bottom). All H-atoms are omitted.

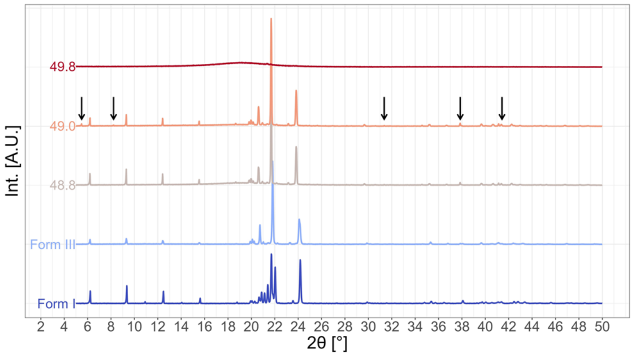

Fig. 12 Powder patterns of MEBE during *in situ* cooling using the Bruker D8 XRD instrument. Peaks characteristic of form II are indicated with black arrows.

capillaries without prior grinding, and the pattern at 25 °C was recorded. The sample was subjected to two heating/cooling cycles. During the first cycle, the sample was heated to 70 °C, at which point the temperature was held for 10 minutes. The sample was then cooled to 25 °C at 1 K min^{-1}. During the second cycle, the sample was heated to 70 °C and held at this temperature for 5 minutes. Following this, it was cooled to 52 °C at 6 K min^{-1}, and then further cooled to 49 °C at a slower cooling rate of ~1 K min^{-1}. The temperature was then held until the crystallisation was completed. Afterwards, the sample was further cooled to 25 °C at 1 K min^{-1}.

First, Pawley refinement of the powder pattern of commercially available MEBE collected at 25 °C was conducted using the structure of form I obtained from the single crystal XRD experiments (Table 5). Fig. 13 shows excellent agreement and again confirms that the commercial sample of MEBE is indeed form I.

On heating (see Fig. A4 in the SI) apart from minor shifts to lower 2*θ* associated with thermal expansion, no phase transitions were observed up to the melting point. Melting commenced at ~56 °C for form I with an overall reduction of peak intensities, and the sample was completely molten by ~59 °C, consistent with the DSC experiments. The slight delay in the endset of melting observed compared to the DSC experiments is most likely caused by lower heat transfer rates in the capillary compared to the DSC furnace.

On cooling from 70 °C (see Fig. A5 in the SI), Bragg peaks first appeared at ~49 °C analogous to the onset of crystallisation observed in the DSC experiment, and was complete by 45 °C. This pattern was consistent with form III with no distinct peaks from form II.

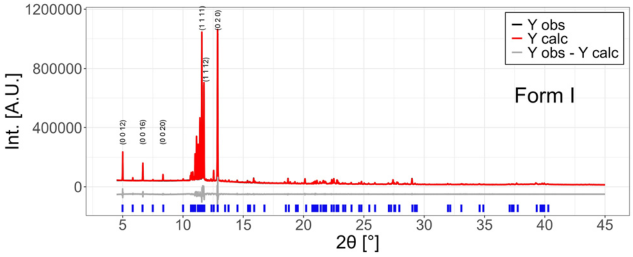

Fig. 13 Pawley fit of PXRD pattern of MEBE at room temperature prior to heating (form I).

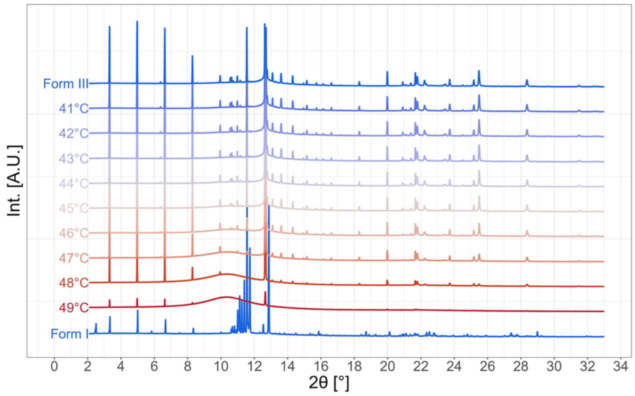

Fig. 14 Powder pattern of MEBE recorded *in situ* at I11 during cooling at 1 K min^{-1}. The curves are colour coded based on the temperatures (blue: colder, red: hotter) and the labels indicate the temperature [°C] at which the pattern was recorded. Int. on the *y*-axis stands for intensity.

This sample was then heated to 70 °C and held at this temperature for 5 minutes (see Fig. A6 in the SI). Form III started to melt at 52 °C and was complete by 57 °C, again consistent with the DSC experimental data.

On cooling to 49 °C (Fig. 14), peaks associated with form III were observed, and again no distinct peaks from form II were noticed.

Pawley refinement of the powder pattern collected at 25 °C showed the presence of phase-pure form III (in the SI).

These observations confirm the highly metastable nature of form II and its very limited range of stability. This is further compounded by the varying experimental conditions, *e.g.* cooling rate, nature of confinement, and X-ray beam intensity.

4 Discussion

These results show that the polymorphic behaviour of MEBE is more complex than expected. Of particular note is the high degree of metastability of form II, which exists only over a very limited temperature range (50.5–49.5 °C). Form I has a higher melting temperature (T_m) and enthalpy of fusion (ΔH) than form III, and therefore is thermodynamically more stable than both forms II and III. The observation that on heating, form III persists without transforming into form I highlights the substantial barrier to interconversion of the two forms. The crystal structures, compounded by the size of the molecules, highlight the significant molecular rearrangement that would be required to convert form III into form I. Also of note is the observation that form I can only be obtained from crystallisation from solution, and not from the melt, at least under the conditions explored here. This suggests a comparatively high nucleation barrier, likely associated with the formation of a more complex critical nucleus, which may be disfavoured in the melt. In contrast, crystallisation from solution may promote aggregation of molecules through specific solvent–solute interactions, facilitating partially ordered arrangements consistent with the bilayer motif observed. This has substantial implications for the use of PCMs in heat storage applications that utilise polymorphic materials, *i.e.* situations where the initial polymorph does not recrystallise after the first or subsequent heating/cooling cycles, thereby compromising the performance of the latent heat storage system.

Liu *et al.*[22] found that differences in the polymorphic behaviour of methyl stearate are mainly influenced by the packing of the terminal methyl groups. This is also true for MEBE, for which form I and form III essentially differ in the packing of end methyl groups in either a head-to-head/tail-to-tail arrangement, which results in oblique layers, or a head-to-tail arrangement, which results in monolayers (Fig. 11).

Form I of MEBE crystallises from solution in the bilayer arrangement similar to form II and form III of methyl stearate, which are also obtained by crystallisation from solution. In contrast, form III of MEBE obtained from the melt comprises monolayers similar to form IV and form V of methyl stearate, which were also grown from the melt. This lends further support to the hypothesis that the bilayers form in solution because of intermolecular hydrophobic interactions.[22]

A few additional considerations can be expressed on the influence of polymorphism on the thermophysical properties of FAMEs and homologues. While extensive studies have correlated polymorphic structure and thermal behaviour in triglycerides, less attention has been placed on FAMEs.[7] Nevertheless, some general trends can provide useful context. For linear, saturated FAMEs, properties such as melting point, enthalpy of fusion, and specific heat capacity increase with increasing chain length. This is typically observed with a near-linear trend for even-numbered chains, while odd-numbered homologues exhibit comparatively lower values. The presence of unsaturated bonds disrupts the packing efficiency, leading to reduced melting points and latent heats, with a more pronounced effect in *cis*- rather than *trans*-configurations. While longer-chain compounds typically exhibit reduced supercooling, very long chains may have steric constraints that hinder nucleation and increase supercooling. Overall, these effects can be associated with the degree of packing efficiency of the hydrocarbon chains.[7,39] Although not yet predictive, such observations contribute to a growing framework in which both molecular structure (*e.g.*, chain length, saturation) and crystallisation conditions influence polymorph selection and, consequently, thermal performance. This highlights the importance of considering both structural and processing factors when developing FAME-based phase change materials.

This study highlights the complementary nature of the three characterisation techniques (DSC, HSM, and PXRD) deployed here. Each provides specific insights into temperature-induced changes in the material, and demonstrates the consistency of thermal events across each technique.

5 Conclusions

This work establishes that methyl behenate (MEBE) is polymorphic and exists in three distinct forms – form I, form II, and form III – whose occurrence depends strongly on thermal history. By combining DSC, hot-stage microscopy, single-crystal and powder X-ray diffraction, and *in situ* synchrotron PXRD, we show that: (i) form I is the thermodynamically stable polymorph under ambient conditions, which exhibits the highest melting point and enthalpy of fusion, and is the polymorph obtained in commercial samples and by crystallisation from solution; (ii) on cooling of the melt, crystallisation proceeds first to give a highly metastable form II that exists within only a very narrow temperature window (~50.5–49.5 °C) before rapidly transforming to form III; and (iii) form III melts on reheating without converting to form I. Thus, once thermally cycled, MEBE behaves as form III, which displays a slightly lower T_m and ΔH than form I. The crystal structures of forms I and III have been determined for the first time. Form I crystallises from solution in the orthorhombic crystal system (space group $Pna2_1$) and the molecules pack as tilted bilayers with head to head/tail to tail arrangements. Form III, obtained from the melt, crystallises in the monoclinic crystal system (space group $C2/c$) and the molecules pack in monolayers with pronounced disorder about a centre of inversion. These structure–property relationships mirror those reported for other long-chain FAMEs, where thermophysical properties are closely linked to hydrocarbon chain packing, methylene subcell symmetry, and the relative orientation of neighbouring chains. In particular, bilayer arrangements with head-to-head/tail-to-tail packing are typically associated with more efficient chain packing and higher T_m and ΔH values, whereas monolayer arrangements exhibit slightly reduced thermodynamic stability. While thermophysical data for comparable polymorphs in other FAMEs are limited, the structural similarities suggest that predictable relationships between packing and thermal properties may exist within this class of compounds. This highlights a potential pathway for controlling polymorphism in PCM systems through the combined selection of molecular structure and crystallisation conditions. From an application standpoint, these findings have direct implications for latent heat storage over the 45–55 °C range using MEBE as the PCM. Thermal stores initially filled with form I are likely to operate as form III after the first melt-recrystallisation cycle, leading to a modest, but systematic shift in melting temperature and stored energy. Reliable PCM performance therefore requires explicit control over polymorph selection and cycling conditions, alongside clear reporting of crystalline form, processing history, and measurement protocols.

6 Outlook

By clarifying the polymorphism of MEBE and its impact on thermophysical properties, this study provides both a structural foundation and practical guidance for deploying polymorphic fatty ester PCMs. The parallels with methyl stearate suggest that rational polymorph control across the FAME family is an attainable route to more predictable and efficient thermal energy storage.

To achieve this, future research efforts should focus on resolving the structure and stability field of form II using time-resolved diffraction (fast synchrotron detectors), microcrystal electron diffraction, and complementary spectroscopic techniques to study its transient nature. Further studies should quantify the nucleation and transformation kinetics as a function of cooling rate, supercooling, and confinement to establish processing conditions for reproducible control of form. Polymorph control strategies that are relevant for deployment should be explored, including templating/seeding (*i.e.* with compounds with similar unit cell parameters and a higher melting point), tailored cooling profiles, confinement/encapsulation, and impurity or additive screening to stabilise desired forms. Predictive structure–property relationships should be developed, supported by MD simulations. Finally, evaluation of long-term cycling stability, supercooling behaviour, and composite formulations should be explored in order to mitigate deterioration of thermal storage performance.

Author contributions

Conceptualisation: R. Ravotti, X. Liu, C. R. Pulham; data curation: R. Ravotti, X. Liu; methodology: R. Ravotti, X. Liu, C. R. Pulham; investigation: R. Ravotti; X. Liu; C. R. Pulham; visualisation: R. Ravotti; supervision: X. Liu, C. R. Pulham, A. Stamatiou; writing – original draft: R. Ravotti; X. Liu; C. R. Pulham; writing – review & editing: R. Ravotti, X. Liu, C. R. Pulham, A. Stamatiou.

Conflicts of interest

There are no conflicts to declare.

Abbreviations

The following symbols and abbreviations are used:

DSC	Differential scanning calorimetry
EtOAc	Ethyl acetate
FAME	Fatty acid methyl esters
HSM	Hot stage microscope
HSLU	Lucerne University of Applied Sciences and Arts
LHS	Latent heat storage
MEBE	Methyl behenate
MeOH	Methanol
PCM	Phase change material
TES	Thermal energy storage
XRD	X-ray diffraction
ΔH	Gravimetric enthalpy of fusion [J g^{-1}]
T_0	Induction point [°C]
T_m	Melting point [°C]
T_c	Solidification point [°C]
λ	Wavelength [Å]

Data availability

The supporting data have been provided as part of the supplementary information (SI).

Supplementary information is available. See DOI: https://doi.org/10.1039/d6ce00065g.

CCDC 2421186 (form I) and 2421158 (form III) contain the supplementary crystallographic data for this paper.[40a,b]

Acknowledgements

The authors would like to thank Sarah Day and Stephen Thompson at the I11 beamline synchrotron facility at the Diamond Light Source, Harwell (UK) for the dynamic *in situ* measurements of methyl behenate.

Notes and references

1 World Energy Transitions Outlook: 1.5 °C Pathway, ed. I. R. E. A. (IRENA), International Renewable Energy Agency (IRENA), Abu Dhabi, 1st edn, 2021.
2 Innovation outlook: Thermal energy storage, ed. I. R. E. A. (IRENA), International Renewable Energy Agency (IRENA), Abu Dhabi, 1st edn, 2020.
3 W. Aftab, A. Usman, J. Shi, K. Yuan, M. Qin and R. Zou, *Energy Environ. Sci.*, 2021, **14**, 4268–4291.
4 V. Tyagi, K. Chopra, R. Sharma, A. Pandey, S. Tyagi, M. Ahmad, A. Sari and R. Kothari, *Sol. Energy Mater. Sol. Cells*, 2022, **234**, 111392.
5 O. Okogeri and V. Stathopoulos, *Int. J. Thermofluids*, 2021, **10**, 100081.
6 R. Ravotti, O. Fellmann, N. Lardon, L. J. Fischer, A. Stamatiou and J. Worlitschek, *Appl. Sci.*, 2018, **8**, 1069.
7 R. Ravotti, J. Wortlischek, C. Pulham and A. Stamatiou, *Molecules*, 2020, **25**(23), 5572.
8 L. Dash and P. Mahanwar, *IJEAST*, 2021, **5**(9), 268–284.
9 R. Ravotti, O. Fellmann, N. Lardon, L. J. Fischer, A. Stamatiou and J. Worlitschek, *Appl. Sci.*, 2019, **9**(2), 225.
10 G. Suppes, M. Goff and S. Lopes, *Chem. Eng. Sci.*, 2003, **58**(9), 1751–1763.
11 J. Bernstein, *Cryst. Growth Des.*, 2011, **11**(3), 632–650.
12 A. Cruz-Cabeza, S. M. Reutzel-Edens and J. Bernstein, *Chem. Soc. Rev.*, 2015, **44**, 8619–8635.
13 S. Gunasekara, C. Barreneche, A. Ines Fernandez, A. Calderon, R. Ravotti, A. Ristic, P. Weinberger, A. Paksoy, B. Kocak, C. Rathgeber, J. Chiu and A. Stamatiou, *Crystals*, 2021, **11**, 1276.
14 E. S. Lutton, *J. Am. Oil Chem. Soc.*, 1945, **67**, 524–527.
15 T. Malkin, *J. Chem. Soc.*, 1940, 1–50.
16 A. Van Langevelde, R. Peschar and H. Schenk, *Acta Crystallogr., Sect. B: Struct. Sci., Cryst. Eng. Mater.*, 2001, **57**, 372–377.

17 P. Duffy, *J. Chem. Soc.*, 1853, 197.

18 J. W. Hagemann and J. A. Rothfus, *J. Am. Oil Chem. Soc.*, 1988, **65**, 638–646.

19 L. Hernqvist, *Food Str.*, 1990, **9**(1), 39–44.

20 L. Hernqvist and K. Larsson, *Fette, Seifen, Anstrichm.*, 1982, **84**(9), 349–354.

21 E. Lutton and F. Hugenberg, *J. Chem. Eng. Data*, 1961, **7**(2), 208–209.

22 X. Liu, A. Gibbs, G. Nichol, C. Tang, P. Knight, K. S. Dowding, I. More and C. Pulham, *CrystEngComm*, 2018, **20**, 6885–6893.

23 S. Cabus, J. Bogaerts, J. Van Mechelen, M. Smet and B. Goderis, *Cryst. Growth Des.*, 2013, **13**(8), 3438–3446.

24 N. Soodoo, K. Poopalam, L. Bouzidi and S. Narine, *Sol. Energy Mater. Sol. Cells*, 2022, **238**, 111650.

25 P. Avato and A. Tava, *Phytochem. Rev.*, 2022, **21**(2), 401–428.

26 Y. Bhutto, A. Pandey, R. Saidur, P. Rathore and M. Samykano, *J. Energy Storage*, 2024, **93**, 112320.

27 J. Pereira da Cunha and P. Eames, *Appl. Energy*, 2016, **177**, 227–238.

28 B. Zalba, J. MarıIn, L. Cabeza and H. Mehling, *Appl. Therm. Eng.*, 2003, **23**(3), 251–283.

29 J. Brubach, V. Jannin, B. Mahler, C. Bourgaux, P. Lessieur, P. Roy and M. Ollivon, *Int. J. Pharm.*, 2007, **336**(2), 248–256.

30 P. Pivette, V. Faivre, J. Brubach, G. Daste, M. Ollivon and S. Lesieur, *Chem. Phys. Lipids*, 2014, **183**, 191–203.

31 H. Takiguchi, J. Yano, T. Nakada, S. Miyashita, H. Komatsu and K. Sato, *J. Cryst. Growth*, 1999, **205**(4), 575–583.

32 https://www.mt.com/ch/it/home/supportive_content/matchar_apps/MatChar_UC232.html.

33 Rigaku Oxford Diffraction, Technol. UK Ltd, Yarnton, Oxford, UK, 2014.

34 O. V. Dolomanov, L. J. Bourhis, R. J. Gildea, J. A. K. Howard and H. Puschmann, *J. Appl. Crystallogr.*, 2009, **42**, 339–341.

35 G. Sheldricka, *Acta Crystallogr., Sect. A: Found. Adv.*, 2014, **71**(1), 3–8.

36 G. Sheldricka, *Acta Crystallogr., Sect. C: Struct. Chem.*, 2014, **71**(1), 3–8.

37 A. Coelho, *J. Appl. Crystallogr.*, 2018, **51**, 210–218.

38 G. Pawley, *J. Appl. Crystallogr.*, 1981, **14**, 357–361.

39 A. Gopinath, K. Sairam, R. Velraj and G. Kumaresan, *Proc. Inst. Mech. Eng., Part D*, 2015, **229**(3), 357–390.

40 (*a*) CCDC 2421158: Experimental Crystal Structure Determination, 2026, DOI: 10.5517/ccdc.csd.cc2m8dw6; (*b*) CCDC 2421186: Experimental Crystal Structure Determination, 2026, DOI: 10.5517/ccdc.csd.cc2m8fs4.